

LJMU Research Online

Yao, Y, Alexander, KD, Lu, W, Somalwar, JJ, Ravi, V, Chornock, R, Margutti, R, Perley, DA, Miller-Jones, JCA, Beniamini, P, A.J, N, Bloom, JS, Christy, CT, Graham, MJ, Groom, SL, Hammerstein, E, Helou, G, Kasliwal, MM, Kulkarni, SR, Laher, RR, Mahabal, AA, Neveu, JRM, Riddle, R, Smith, R and van Velzen, S

Optically Overluminous Tidal Disruption Events: Outflow Properties and Implications for Extremely Relativistic Disruptions

https://researchonline.ljmu.ac.uk/id/eprint/27567/

Article

Citation (please note it is advisable to refer to the publisher's version if you intend to cite from this work)

Yao, Y, Alexander, KD, Lu, W, Somalwar, JJ, Ravi, V, Chornock, R, Margutti, R, Perley, DA ORCID logoORCID: https://orcid.org/0000-0001-8472-1996, Miller-Jones, JCA, Beniamini, P, A.J, N, Bloom, JS, Christy, CT, Graham, MJ, Groom. SL. Hammerstein. E. Helou. G. Kasliwal. MM. Kulkarni. SR. Laher.

LJMU has developed **LJMU Research Online** for users to access the research output of the University more effectively. Copyright © and Moral Rights for the papers on this site are retained by the individual authors and/or other copyright owners. Users may download and/or print one copy of any article(s) in LJMU Research Online to facilitate their private study or for non-commercial research. You may not engage in further distribution of the material or use it for any profit-making activities or any commercial gain.

The version presented here may differ from the published version or from the version of the record. Please see the repository URL above for details on accessing the published version and note that access may require a subscription.

For more information please contact researchonline@ljmu.ac.uk





LJMU Research Online

Yao, Yuhan, Alexander, Kate D., Lu, Wenbin, Somalwar, Jean J., Ravi, Vikram, Chornock, Ryan, Margutti, Raffaella, Perley, Daniel A., Miller-Jones, James C. A., Beniamini, Paz, A.J., Nayana, Bloom, Joshua S., Christy, Collin T., Graham, Matthew J., Groom, Steven L., Hammerstein, Erica, Helou, George, Kasliwal, Mansi M., Kulkarni, S. R., Laher, Russ R., Mahabal, Ashish A., Neveu, Jérémy, Riddle, Reed, Smith, Roger and van Velzen, Sjoert

Optically Overluminous Tidal Disruption Events: Outflow Properties and Implications for Extremely Relativistic Disruptions

https://researchonline.ljmu.ac.uk/id/eprint/27494/

Article

Citation (please note it is advisable to refer to the publisher's version if you intend to cite from this work)

Yao, Yuhan ORCID logoORCID: https://orcid.org/0000-0001-6747-8509, Alexander, Kate D. ORCID logoORCID: https://orcid.org/0000-0002-8297-2473, Lu, Wenbin ORCID logoORCID: https://orcid.org/0000-0002-1568-7461, Somalwar. Jean J. ORCID logoORCID: https://orcid.org/0000-0001-8426-

LJMU has developed LJMU Research Online for users to access the research output of the University more effectively. Copyright © and Moral Rights for the papers on this site are retained by the individual authors and/or other copyright owners. Users may download and/or print one copy of any article(s) in LJMU Research Online to facilitate their private study or for non-commercial research. You may not engage in further distribution of the material or use it for any profit-making activities or any commercial gain.

The version presented here may differ from the published version or from the version of the record. Please see the repository URL above for details on accessing the published version and note that access may require a subscription.

For more information please contact $\underline{researchonline@ljmu.ac.uk}$ http://researchonline.ljmu.ac.uk/

OPEN ACCESS



Optically Overluminous Tidal Disruption Events: Outflow Properties and Implications for Extremely Relativistic Disruptions

```
Yuhan Yao<sup>1,2,3</sup>, Kate D. Alexander<sup>4</sup>, Wenbin Lu<sup>2,3,5</sup>, Jean J. Somalwar<sup>6</sup>, Vikram Ravi<sup>6</sup>, Ryan Chornock<sup>2,3</sup>, Raffaella Margutti<sup>2,3,7</sup>, Daniel A. Perley<sup>8</sup>, James C. A. Miller-Jones<sup>9</sup>, Paz Beniamini<sup>10,11,12</sup>, Nayana A.J.<sup>2,3</sup>, Joshua S. Bloom<sup>2,3,13</sup>, Collin T. Christy<sup>4</sup>, Matthew J. Graham<sup>6</sup>, Steven L. Groom<sup>14</sup>, Erica Hammerstein<sup>2,3</sup>,
George Helou<sup>14</sup>, Mansi M. Kasliwal<sup>6</sup>, S. R. Kulkarni<sup>6</sup>, Russ R. Laher<sup>14</sup>, Ashish A. Mahabal<sup>6,15</sup>, Jérémy Neveu<sup>16</sup>,
                                                                                               Reed Riddle 17, Roger Smith 17, and Sjoert van Velzen 18, and Sjoert v
                                               <sup>1</sup> Miller Institute for Basic Research in Science, 206B Stanley Hall, Berkeley, CA 94720, USA; yuhanyao@berkeley.edu
                                                                                         Department of Astronomy, University of California, Berkeley, CA 94720-3411, USA
    <sup>3</sup> Berkeley Center for Multi-messenger Research on Astrophysical Transients and Outreach (Multi-RAPTOR), University of California, Berkeley, CA 94720-
                                                                                                                                                                             3411, USA
                                            <sup>4</sup> Department of Astronomy/Steward Observatory, 933 North Cherry Avenue, Room N204, Tucson, AZ 85721-0065, USA
      Theoretical Astrophysics Center, University of California, Berkeley, CA 94720, USA

Cahill Center for Astronomy and Astrophysics, California Institute of Technology, MC 249-17, 1200 E California Boulevard, Pasadena, CA 91125, USA

Department of Physics, University of California, 366 Physics North MC 7300, Berkeley, CA 94720, USA
                    8 Astrophysics Research Institute, Liverpool John Moores University, IC2, Liverpool Science Park, 146 Brownlow Hill, Liverpool L3 5RF, UK
                                                   International Centre for Radio Astronomy Research, Curtin University, GPO Box U1987, Perth, WA 6845, Australia <sup>10</sup> Department of Natural Sciences, The Open University of Israel, P.O. Box 808, Ra'anana 4353701, Israel
                          Astrophysics Research Center of the Open University (ARCO), The Open University of Israel, P.O. Box 808, Ra'anana 4353701, Israel
                                                            Department of Physics, The George Washington University, 725 21st Street NW, Washington, DC 20052, USA
                                                                      Lawrence Berkeley National Laboratory, 1 Cyclotron Road, MS 50B-4206, Berkeley, CA 94720, USA
                                                                              <sup>1</sup> IPAC, California Institute of Technology, 1200 E. California Blvd, Pasadena, CA 91125, USA
                                                                      15 Center for Data Driven Discovery, California Institute of Technology, Pasadena, CA 91125, USA

16 Université Paris-Saclay, CNRS, IJCLab, 91405, Orsay, France
                                                                           <sup>17</sup> Caltech Optical Observatories, California Institute of Technology, Pasadena, CA 91125, USA <sup>18</sup> Leiden Observatory, Leiden University, Postbus 9513, 2300 RA, Leiden, The Netherlands
                                                         Received 2025 June 17; revised 2025 September 11; accepted 2025 September 16; published 2025 November 5
```

Abstract

Recent studies suggest that tidal disruption events (TDEs) with off-axis jets may manifest as optically overluminous events. To search for jet signatures at late times, we conducted radio observations of eight such optically overluminous ($M_{g,peak} < -20.8$ mag) TDEs with the Very Large Array. We detect radio counterparts in four events. The observed radio luminosities ($L_{6~\rm GHz} \sim 10^{38}$ – 10^{39} erg s⁻¹) are two orders of magnitude lower than those of on-axis jetted TDEs, and we find no evidence for off-axis jets within a rest-frame time of 3 yr. Two of them (AT2022hvp and AT2021aeou) exhibit evolving radio emission, consistent with synchrotron emission from non-relativistic outflows launched near the time of first optical light. Two events (AT2020ysg and AT2020qhs) show no statistically significant variability, which can be attributed to either non-relativistic outflows or pre-existing active galactic nuclei. Compared to a control sample of fainter TDEs with $M_{g,peak} > -20.5$ mag observed at similar rest-frame timescales ($t_{\rm rest} \sim 1.5$ yr), our sample shows systematically more luminous radio emission, suggesting that optically overluminous TDEs may launch more powerful prompt non-relativistic outflows. We speculate that strong general relativistic effects near high-mass black holes ($M_{\rm BH} \sim 10^8 \, M_{\odot}$) may play a key role. These findings motivate further investigation into the nature of relativistic disruptions around massive black holes and the physical conditions necessary for jet formation.

Unified Astronomy Thesaurus concepts: Tidal disruption (1696); Radio transient sources (2008); Time domain astronomy (2109); Supermassive black holes (1663)

1. Introduction

Tidal disruption events (TDEs) are rare electromagnetic transients where a star is torn apart by the tidal forces of a massive black hole. In some cases, such events are accompanied by the ejection of material in the form of collimated relativistic jets, which emit prompt X-ray light and lower frequency afterglows (see K. D. Alexander et al. 2020; F. De Colle & W. Lu 2020 for reviews). So far, only four on-axis jetted TDEs have been identified, including Sw J1644+57¹⁹ (J. S. Bloom

Original content from this work may be used under the terms of the Creative Commons Attribution 4.0 licence. Any further distribution of this work must maintain attribution to the author(s) and the title of the work, journal citation and DOI.

et al. 2011; D. N. Burrows et al. 2011; A. J. Levan et al. 2011; B. A. Zauderer et al. 2011), Sw J2058+05 (S. B. Cenko et al. 2012; D. R. Pasham et al. 2015), Sw J1112-82 (G. C. Brown et al. 2015, 2017), and AT2022cmc (I. Andreoni et al. 2022; D. R. Pasham et al. 2023). The volumetric rate of on-axis jetted TDEs is found to be 0.01–0.07 Gpc⁻³ yr⁻¹ (H. Sun et al. 2015; I. Andreoni et al. 2022). Assuming a relativistic beaming factor of $f_b \approx 0.01$, the intrinsic rate of jetted TDEs²⁰ (1–7 Gpc⁻³ yr⁻¹) appears to be a tiny fraction ($\leq 0.1\%$ –1%) of the total TDE rate of $\sim 10^3$ Gpc⁻³ yr⁻¹ (S. Sazonov et al. 2021; Y. Yao et al. 2023; M. Masterson et al. 2024). It is possible that misaligned precessing jets can be choked by the accretion disk wind (O. Teboul & B. D. Metzger 2023; W. Lu et al. 2024).

¹⁹ We note that an alternative interpretation is that Sw J1644+57 harbors a slightly off-axis jet (P. Beniamini et al. 2023).

²⁰ Strictly speaking, this refers to TDEs with prompt relativistic jets. In this paper, we do not consider the possibility of relativistic jets launched significantly after disruption.

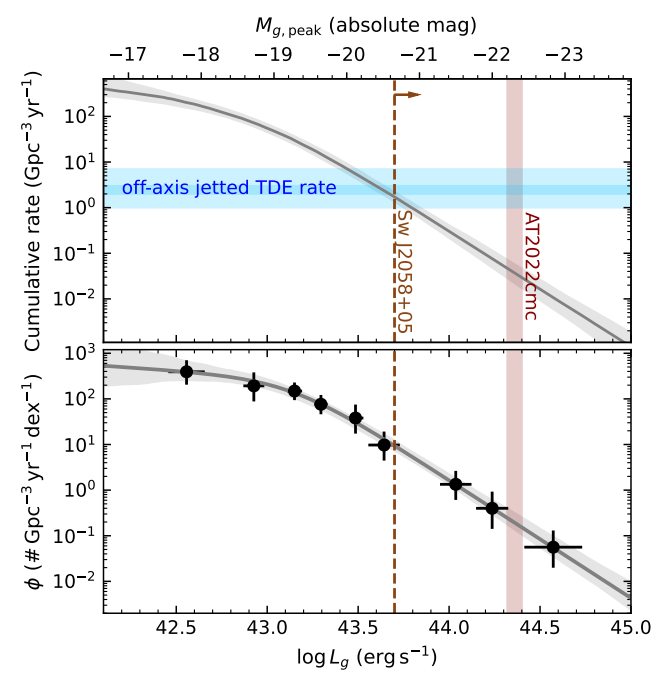


Figure 1. Cumulative optical TDE rate (upper panel) and rest-frame *g*-band ($\nu_{\rm rest} = 6.3 \times 10^{14}$ Hz) luminosity function (bottom panel; Y. Yao et al. 2023). The vertical lines mark the peak L_g of two on-axis jetted TDEs (D. R. Pasham et al. 2015; I. Andreoni et al. 2022; Y. Yao et al. 2024).

In the UV and optical band, the TDE population spans a wide range of peak luminosities and spectral subtypes (S. van Velzen et al. 2020). Based on the existence of broad (full width at half-maximum of $>5 \times 10^3 \, \mathrm{km \, s^{-1}}$) emission lines, S. van Velzen et al. (2021) proposed a classification scheme dividing TDEs into three subclasses: TDE-H, TDE-He, and TDE-H +He. More recently, E. Hammerstein et al. (2023b) identified four TDEs with high luminosities and featureless optical spectra, and additional similar events have been reported by Y. Yao et al. (2023). While many of these overluminous TDEs lack spectral features, some do exhibit broad lines (e.g., see H. Kumar et al. 2024 and Section 2). Conversely, there are also examples of optically subluminous TDEs with featureless spectra (e.g., Y. Yao et al. 2022).

I. Andreoni et al. (2022) suggested the possibility that the population of off-axis jetted TDEs might manifest themselves as slowly evolving, overluminous, featureless blue nuclear transients in optical sky surveys. This hypothesis is based on observations of known on-axis jetted TDEs. In both Sw J2058 +05 (D. R. Pasham et al. 2015) and AT2022cmc (I. Andreoni et al. 2022; Y. Yao et al. 2024; E. Hammerstein et al. 2025), the peak (rest-frame) UV and optical spectral energy distribution (SED) has been observed. Both events exhibit thermal SEDs that can be described by a blackbody with low values of $M_{g,peak}$, which correspond to high luminosities (see Figure 1). They also show featureless spectra. Further evidence comes from the volumetric rate of optically overluminous TDEs, which is a few × Gpc^{-3} yr⁻¹ (see Figure 1)—a rate consistent with expectations for off-axis jetted TDEs.

In this work, we test this hypothesis using late-time radio observations of eight optically overluminous TDEs discovered by the Zwicky Transient Facility (ZTF; E. C. Bellm et al. 2019; M. J. Graham et al. 2019; F. J. Masci et al. 2019; R. Dekany et al. 2020). In the off-axis jet scenario, radio emission is expected to peak on a timescale that depends on

viewing angle and eventually resemble the light curve of an on-axis jet (P. Beniamini et al. 2020; G. Ryan et al. 2020). Therefore, if most optically overluminous TDEs harbor off-axis relativistic jets, their late-time radio luminosities should be comparable to those of known jetted TDEs.

UT time is used throughout the paper. We adopt a standard Λ CDM cosmology with $\Omega_{\rm M}=0.3,~\Omega_{\Lambda}=0.7$, and $H_0=70\,{\rm km\,s^{-1}\,Mpc^{-1}}$. Uncertainties are reported at the 68% confidence intervals unless otherwise noted, and upper limits are reported at 3σ .

2. Sample Selection and Observations

We collected all TDEs that were first detected by ZTF from 2019 January 1 to 2022 May 1, resulting in 62 events. The TDEs were photometrically selected using a custom filter (S. van Velzen et al. 2021) built upon the AMPEL broker (J. Nordin et al. 2019), and spectroscopically classified. We modeled their UV–optical light curves and host galaxies using the procedures outlined in Y. Yao et al. (2023). The best-fit light curve model provides peak rest-frame g-band absolute magnitude $M_{g,peak}^{21}$ and the functional form (power law or Gaussian) that best describes the rising part of the light curves. For a power-law rise, the first-light epoch $t_{\rm fl}$ is given by the best-fit model. For a Gaussian rise, we define $t_{\rm fl} \equiv t_{\rm peak} - 3\sigma_{\rm rise}$, where $t_{\rm peak}$ is the time of the optical peak and $\sigma_{\rm rise}$ is the Gaussian rise time. Hereafter, we use $t_{\rm rest}$ to denote rest-frame time with respect to $t_{\rm fl}$.

Figure 2 shows the distribution of 62 TDEs on the panel of redshift versus $M_{g,peak}$. Figure 3 shows the host galaxy total stellar mass M_{gal} versus Galactic extinction-corrected, synthetic rest-frame u-r color. A total of 11 TDEs have $M_{g,peak} < -20.8$ mag. The threshold of -20.8 mag is a somewhat arbitrary cut to separate overluminous and normal-luminosity events, as the luminosity function is a continuous power law in this range (see Figure 1). As can be seen, due to the small intrinsic rate of overluminous TDEs, they are generally selected at much higher redshifts (z>0.1) and were mostly missed by previous radio TDE follow-up programs (e.g., K. D. Alexander et al. 2025). We selected eight objects spanning a range of $M_{g,peak}$ with different spectroscopic and light curve shapes for radio observations.

Basic properties of the sample are summarized in Table 1. Our sample spans a range of $M_{g,\mathrm{peak}}$ and various spectral subtypes. Figure 4 shows their ZTF r-band light curves obtained through forced photometry (F. J. Masci et al. 2023). As can be seen, most of them exhibit a late-time plateau that has been uniquely observed in TDEs (A. Mummery et al. 2024).

We adopt the spectroscopic classification nomenclature introduced in S. van Velzen et al. (2021), E. Hammerstein et al. (2023b), and Y. Yao et al. (2023), where optical TDEs are divided into five subtypes: TDE-H, TDE-He, TDE-H+He, TDE-featureless, and TDE-coronal. In our sample, five objects (AT2020ysg, AT2021yzv, AT2020acka, AT2020qhs, AT2019cmw) have been previously reported as TDEs with assigned subtypes in refereed articles (E. Hammerstein et al. 2023b; Y. Yao et al. 2023), two objects (AT2022hvp, AT2021gje) have been reported to the transient name server

 $[\]overline{^{21}}$ For light curves with multiple peaks, $M_{g, \text{peak}}$ is measured for the most luminous peak.

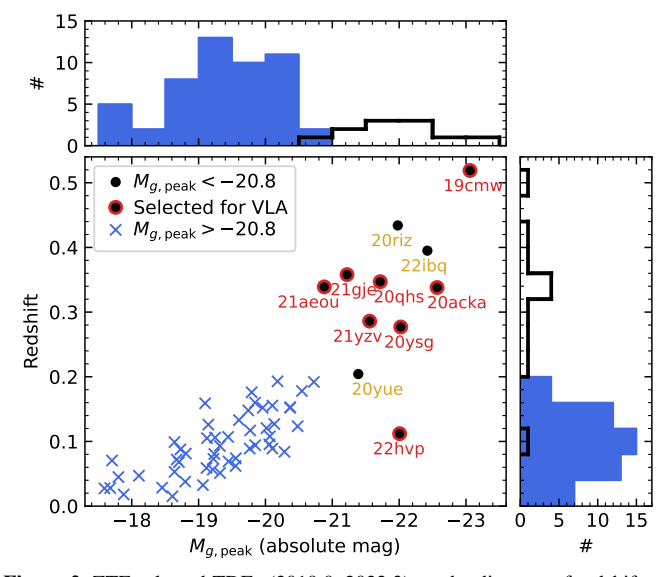


Figure 2. ZTF-selected TDEs (2019.0–2022.3) on the diagram of redshift vs. peak rest-frame *g*-band absolute magnitude. Overluminous TDEs selected for Very Large Array (VLA) observations are annotated.

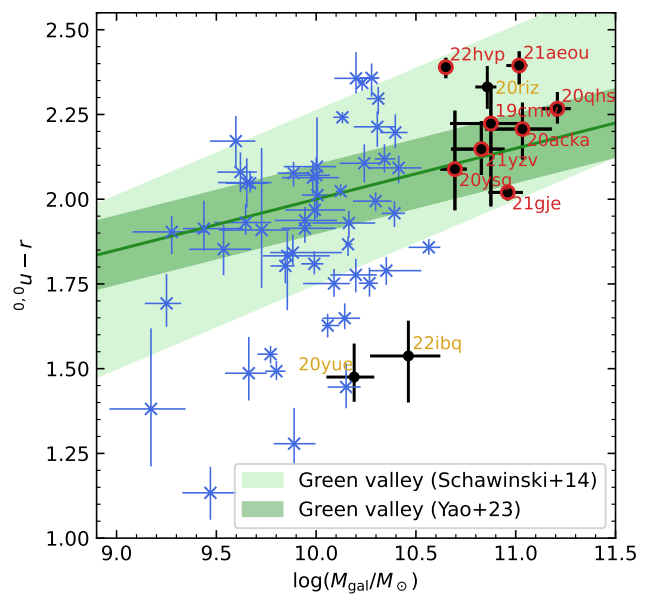


Figure 3. The same sample as in Figure 2, but in the galaxy color–mass diagram. TDEs selected for Very Large Array observations are hosted by higher-mass galaxies.

(TNS) as TDEs (E. Hammerstein 2021; M. Fulton et al. 2022), and AT2021aeou has not been classified before.

An in-depth study of AT2019cmw has been presented by J. Wise et al. (2025), and the optical spectral observations of AT2019cmw will be presented by W. Wu et al. (2025, in preparation). For three objects (AT2022hvp, AT2020ysg, and AT2021aeou), we present optical spectroscopy in Appendix B, which supports the TDE redshift and subtype classification shown in Table 1.

We obtained radio observations using NSF's Karl G. Jansky Very Large Array (VLA; R. A. Perley et al. 2011). The search epoch is conducted in C-band under program 23A-280 (PI: Y. Yao). Follow-up observations for four detected TDEs are obtained through programs 23A-413 and 24A-290 (PI: Y. Yao). We also include data of AT2022hvp obtained under the VLA large program 20B-377 (PI: K. D. Alexander). The

data were analyzed following the standard radio continuum image analysis procedures in the Common Astronomy Software Applications (CASA; CASA Team et al. 2022). We used tclean to produce radio images. The flux density was measured as the maximum pixel value within a region with the size of the synthesized beam, centered on the optical coordinates of the TDE. The uncertainty was estimated as the rms of the pixel values in a nearby source-free region of the image. The results are presented in Appendix C (Table 6).

3. Non-relativistic Outflow Modeling

Figure 5 presents the 6 GHz C-band light curves and upper limits for our sample, alongside a comparison with well-studied TDEs from the literature. Four objects (AT2021yzv, AT2020acka, AT2021gje, and AT2019cmw) are not detected. We perform spectral fitting to assess whether or not the four events with detected radio emission are consistent with synchrotron self-absorption expected in a newly launched non-relativistic TDE outflow.

We assume the electrons in the shock are accelerated into a power-law distribution, $N(\gamma_{\rm e}) \propto \gamma_{\rm e}^{-p}$ for $\gamma_{\rm e} \geqslant \gamma_{\rm m}$, where $\gamma_{\rm m}$ is the minimum Lorentz factor of the relativistic electrons. A fraction $\epsilon_{\rm e}$ of the shock energy goes into relativistic electrons, and a fraction $\epsilon_{\rm B}$ of the shock energy goes into magnetic energy density. The critical electron Lorentz factor at which synchrotron cooling time equals the dynamical time is $\gamma_{\rm c}$. The characteristic synchrotron frequencies for electrons with $\gamma_{\rm e} = \gamma_{\rm m}$ and $\gamma_{\rm e} = \gamma_{\rm c}$ are denoted as $\nu_{\rm m}$ and $\nu_{\rm c}$, respectively. The self-absorption frequency is denoted as $\nu_{\rm a}$, below which the system is optically thick to its own synchrotron emission.

We assume that $\nu_{\rm p}$ is associated with $\nu_{\rm a}$ (i.e., $\nu_{\rm m} \ll \nu_{\rm a} = \nu_{\rm p} \ll \nu_{\rm c}$), which is generally the case for a non-relativistic outflow. The radio SED follows a smoothed power law:

$$L_{\nu} = L_{\nu,p} \left[\left(\frac{\nu}{\nu_{p}} \right)^{-s\beta_{1}} + \left(\frac{\nu}{\nu_{p}} \right)^{-s\beta_{2}} \right]^{-1/s} \tag{1}$$

where ν and L_{ν} are quantities in the object's rest-frame, $\beta_1 = 5/2$ and $\beta_2 = -(p-1)/2$ are the asymptotic spectral indices below and above the break, and s = 1.25 - 0.18p is a smoothing parameter (J. Granot & R. Sari 2002).

For AT2022hvp and AT2021aeou, there are epochs where the peak specific luminosity $L_{\nu,p}$ and the peak frequency ν_p can be reliably measured (see Figure 6). This enables a direct constraint on the equipartition energy ($E_{\rm eq}$) of the outflow at individual epochs. As we will show in Section 3.1, $E_{\rm eq}$ is consistent with remaining constant in both events.

For AT2020ysg and AT2020qhs, the data are much sparser, and $L_{\nu,p}$, and ν_p cannot be well constrained (see Figure 7). To reduce the number of free model parameters, we assume that their outflows are in the Sedov–Taylor (ST) phase where energy is conserved, and adopt a density profile for the surrounding medium of the form $n(r) \propto r^{-k}$. We note that this model does not apply if there are late-time energy injections from the TDE accretion flow.

3.1. AT2020hvp and AT2021aeou

We fit broken power laws to the SEDs using the Markov Chain Monte Carlo (MCMC) approach with emcee (D. Foreman-Mackey et al. 2013). Both detections and non-detections are incorporated in the fitting following the procedures outlined in

Table 1

Basic Information of Eight Optically Overluminous TDEs Selected for VLA Observations

IAU Name	ZTF Name	Redshift	TDE Report	Spectral Subtype	$M_{g,\mathrm{peak}}$	t _{fl} MJD	σ_*^{c} (km s ⁻¹)	$\frac{\log M_{\rm BH}^{\ c}}{(M_{\odot})}$
AT2022hvp	ZTF22aagyuao	0.112	M. Fulton et al. (2022)	TDE-He ^a	-22.01	59676.3	134.96 ± 11.03	7.74 ± 0.34
AT2020ysg	ZTF20abnorit	0.277	E. Hammerstein et al. (2023b)	TDE-He ^a	-22.02	59015.3	157.78 ± 13.03	8.04 ± 0.33
AT2021yzv	ZTF21abxngcz	0.286	Y. Yao et al. (2023)	TDE-featureless	-21.56	59435.3	146.38 ± 20.78	7.90 ± 0.40
AT2020acka	ZTF20acwytxn	0.338	Y. Yao et al. (2023)	TDE-featureless	-22.57	59125.8	174.47 ± 25.30	8.23 ± 0.40
AT2021aeou	ZTF21abvpudz	0.339	This paper	TDE-featureless ^a	-20.88	59439.5		8.30 ± 0.83
AT2020qhs	ZTF20abowque	0.347	E. Hammerstein et al. (2023b)	TDE-featureless	-21.72	58945.1	188.69 ± 37.86	$8.38 ~\pm~ 0.48$
AT2021gje	ZTF21aapvvtb	0.358	E. Hammerstein (2021)	TDE-He-pec ^b	-21.22	59240.5	132.00 ± 8.55	$7.70 ~\pm~ 0.32$
AT2019cmw	ZTF19aaniqrr	0.519	Y. Yao et al. (2023)	TDE-featureless	-23.06	58558.3		$8.07 ~\pm~ 0.87$

Notes.

T. Laskar et al. (2014) and T. Eftekhari et al. (2024). For AT2022hvp, we fix the value of p to be the same across different epochs. Due to the partial SED coverage in AT2021aeou, we fix p = 2.7 (see K. D. Alexander et al. 2016; Y. Cendes et al. 2021; A. J. Goodwin et al. 2022).

The best-fit models are plotted in Figure 6, with model parameters (ν_p , $L_{\nu,p}$, and p) presented in Table 2. Assuming that the outflow is launched around the time of optical first light, we can infer physical properties of the outflow and ambient environment. Following previous TDE radio studies (Y. Cendes et al. 2022; C. T. Christy et al. 2024; A. J. Goodwin et al. 2025a), we adopt the equipartition ($\epsilon_e = \epsilon_B = 0.1$) derivations of R. Barniol Duran et al. (2013) and assume a spherical geometry of the outflow (see Equations (4)–(13) in A. J. Goodwin et al. 2022). The equipartition energy (E_{eq}) and radius (R_{eq}) are the minimum values—deviations from equipartition will render the parameters larger. The inferred parameters are shown in Table 2. The inferred E_{eq} , β , and M_{ej} are on the high end of those of X-ray (eROSITA) selected TDEs (A. J. Goodwin et al. 2025a). We discuss the comparison with optically selected TDEs in Section 4.3.

3.2. AT2020ysg and AT2020qhs

In the ST phase, and assuming $n(r) \propto r^{-k}$, the outflow velocity follows $\beta \propto t^{(k-3)/(5-k)}$, and both $L_{\nu,p}$ and ν_p can be solved as functions of $t_{\rm rest}$. Due to the paucity of data for these two sources, we fix p=2.7. We assign flat priors: $0 \leqslant k \leqslant 2.99$, $-3 \leqslant \log \beta_{2.5 \ \rm yr} \leqslant -1$, where $\beta_{2.5 \ \rm yr}$ is the outflow velocity at $t_{\rm rest}=2.5$ yr. For AT2020qhs, we further assume that the C-band light curve is in the optically thin regime, as is the case in other radio-detected TDEs with multi-band observations.

The best-fit parameters are presented in Table 3, and the corresponding models are overplotted on the data in Figure 7. There exists a degeneracy between the inferred outflow velocity and energy. The best-fit value of k approaches the lower bound of the allowed range, reflecting the fact that the observed radio light curve remains flat rather than declining with time. This may indicate that the radio-emitting region is experiencing a moderate amount of late-time energy injection from delayed outflows (not accounted for in our model) or pre-existing accretion activity (see Section 4.1).

Assuming that the outflow entered into the ST phase at time $t_{\rm ST}$, we can compute the ejecta mass in the TDE outflow to be $M_{\rm ej} \sim 10^{-2.2} \, M_{\odot} \times (\beta_{2.5 \, \rm yr}/0.03)^{-0.54} \, (t_{\rm ST}/1 \, \rm yr)^{1.09}$ for

AT2020ysg and $M_{\rm ej} \sim 10^{-2.0} M_{\odot} \times (\beta_{2.5 \, \rm yr}/0.03)^{-0.55}$ $(t_{\rm ST}/1 \, \rm yr)^{1.07}$ for AT2020qhs. We see that the amount of ejecta mass and total energy needed is within the budget expected in a TDE outflow.

4. Discussion

4.1. AGN Contribution

We discuss the possibility that the radio emission of AT2020ysg and AT2020qhs is powered by pre-existing active galactic nuclei (AGN). Assuming a canonical AGN spectral shape of $f_{\nu} \propto \nu^{-0.7}$ (J. J. Condon et al. 2002), their 1.4 GHz luminosity would be $\sim 10^{22.1} \, \mathrm{W \, Hz^{-1}}$, and their 150 MHz luminosity would be $\sim 10^{22.8} \, \mathrm{W \, Hz^{-1}}$. If the host galaxies of AT2020ysg and AT2020qhs indeed harbor AGN with such radio power, the absence of narrow emission lines in their optical spectra (see Appendix B.1 and E. Hammerstein et al. 2023b) would be consistent with expectations, as massive radio AGN host galaxies are typically quiescent systems (R. M. J. Janssen et al. 2012; G. Jin et al. 2025).

Around $M_{\rm gal} \sim 10^{11}\,M_{\odot}$ (i.e., the typical host galaxy mass of our sample, see Figure 3), $\sim 3\%$ of galaxies harbor AGN with $L_{\nu,1.4\,\rm GHz} \geqslant 10^{22.1}\,\rm W\,Hz^{-1}$ (P. N. Best et al. 2005; J. Sabater et al. 2019). This fraction shows no significant redshift evolution (R. Kondapally et al. 2025). Assuming that TDEs occur uniformly across all galaxy types, the probabilities of having zero, one, two, and more than two out of eight TDEs occurring in radio-loud AGN are 78.4%, 19.4%, 2.1%, and 0.1%, respectively. Therefore, although we cannot rule out the possibility that the detected radio emission of both AT2020ysg and AT2020qhs come from pre-existing AGN, this probability is low.

Alternatively, the TDE rate may be enhanced in radio-bright galaxies. Recent work by K. Kaur & N. C. Stone (2025) investigates how the axisymmetric gravitational potential of a massive AGN disk can enhance TDE rates. In their model, the TDE rates are enhanced in AGN with massive gas disks, where $M_{\rm disk} \sim 0.1 M_{\rm BH}$. Similar to the standard scenario (N. C. Stone & B. D. Metzger 2016), most of the TDEs are channeled by highly eccentric orbits near the radius of influence of the central massive black hole:

^a See the optical spectra presented in Appendix B.

b AT2021gje exhibits peculiar optical spectral properties. Detailed analysis will be presented in W. Wu et al. (2025, in preparation).

^c See Appendix A for the methods to estimate velocity dispersion σ_* and black hole mass $M_{\rm BH}$. We note that our $M_{\rm BH}$ are estimated using host galaxy scaling relations.

 $^{^{\}overline{22}}$ To produce a radio luminosity of $\gtrsim 10^{38}$ erg s⁻¹ via star formation, the required star formation rate would be $\gtrsim 2.1~M_{\odot}~\rm yr^{-1}$, which is not consistent with host galaxy population synthesis analysis. Therefore, star formation is unlikely to be the source of the radio emission.

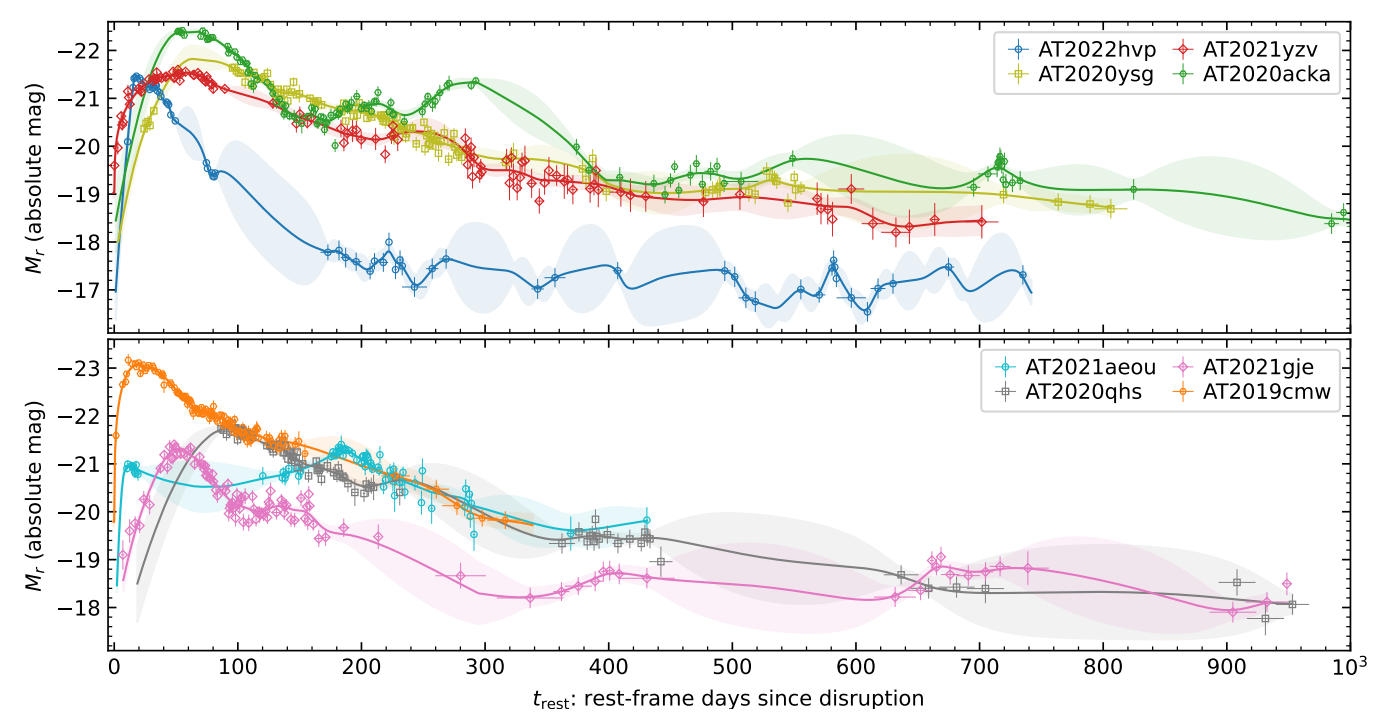


Figure 4. ZTF r-band light curves of our sample. We assume that disruption occurs at the first-light epoch (t_0) . To guide the eye in tracking the light curve evolution, we fit the data using a combination of functional forms and Gaussian process smoothing, following procedures described in Appendix B.4 of Y. Yao et al. (2020). The best-fit models are shown as solid lines, with the 68% confidence intervals displayed in transparent colors. Absolute magnitude is computed using $M = m - 5 \log_{10}[D_L/(10 \text{ pc})] + 2.5 \log_{10}(1 + z)$, where the last term is a rough estimation of the K-correction.

 $r_{\rm h}\approx 10\,{\rm pc}(M_{\rm BH}/10^8\,M_\odot)[\sigma_*/(200\,{\rm km~s^{-1}})]^{-2}$. However, jet-mode (radio-bright) AGN typically have much lower disk masses than radiative-mode AGN (T. M. Heckman & P. N. Best 2014; F. Yuan & R. Narayan 2014), potentially limiting this enhancement mechanism.

A different explanation for the preference of TDEs in jet-mode AGN may be related to black hole spin. Around the black hole mass of our sample ($M_{\rm BH} \sim 10^8\,M_{\odot}$; see Table 1), a Sun-like star can be more easily disrupted if the BH spin is high (M. Kesden 2012; H.-T. Huang & W. Lu 2024; A. Mummery 2024). Moreover, higher-spin black holes are more efficient at launching relativistic jets (A. Tchekhovskoy et al. 2010), providing a natural connection between enhanced spin, higher TDE rates, and stronger radio emission.

4.2. No Evidence of Relativistic Jets

If any of the detected sources in our sample were associated with an off-axis relativistic jet launched at optical discovery with physical properties similar to those of on-axis jetted TDEs, we would expect one of the following observational signatures: (1) a declining light curve with luminosities comparable to those of on-axis jetted TDEs at similar epochs, or (2) a rising radio light curve (see Table A1 of P. Beniamini et al. 2023 for all the possible rise slopes). None of these signatures is observed. Therefore, there is no evidence for off-axis relativistic jets in our sample up to $t_{\rm rest} \sim 3$ yr.

Studies of known on-axis jetted TDEs showed that they are produced by black holes with $M_{\rm BH} \ll 10^8 M_{\odot}$, based on information about host galaxy, X-ray variability timescale, and jet turn-off time inferred from X-ray light curves (see discussion in Section 3.4 of T. Eftekhari et al. 2024). However, it is possible that TDEs hosted by $\sim 10^8 M_{\odot}$ black holes in our sample are preferentially highly spinning (M. Kesden 2012; H.-T. Huang &

W. Lu 2024), which would favor the formation of a powerful jet (A. Tchekhovskoy et al. 2010). Our non-detection of off-axis jets in our sample may be physically explained by the fact that the peak fallback rate of the stellar debris $\dot{M}_{\rm fb,peak} \propto M_{\rm BH}^{-1/2}$ drops below the Eddington limit $\dot{M}_{\rm Edd} \simeq 10 L_{\rm Edd}/c^2 \propto M_{\rm BH}$ at high black hole mass, as the ratio between the two is roughly given by $\dot{M}_{\rm fb,peak}/\dot{M}_{\rm Edd} \simeq 1~(M_*/M_\odot)(M_{\rm BH}/3 \times 10^7 M_\odot)^{-3/2}$ for a mainsequence star of mass M_* (J. A. P. Law-Smith et al. 2020). It has been argued that sub-Eddington, geometrically thin disks do not launch relativistic jets (A. Tchekhovskoy et al. 2014). Our observations are consistent with this theoretical expectation.

In Figure 5, we show example jetted TDE radio light curves for different viewing angle $\theta_{\rm obs}$, assuming all other model parameters follow the best-fit model inferred for Sw J1644 by P. Beniamini et al. (2023). These other parameters include properties associated with the jet (isotropic equivalent kinetic energy $E_{k,iso}$, initial Lorentz factor Γ_0 , angular width θ_0), microphysics $(p, \epsilon_e, \epsilon_B)$, and the surrounding environment (the power-law index of the external density and its normalization). Note that the shape of the radio light curves could change a lot based on the assumed physical parameters. It is therefore possible that the radio emission from off-axis jets only stands out at later time $t_{\text{rest}} > 3 \text{ yr.}$ For instance, AT2018hyz, which has been proposed to harbor a powerful off-axis jet (T. Matsumoto & T. Piran 2023; I. Sfaradi et al. 2024), showed dramatic late-time radio rebrightening with luminosities only becoming comparable to those of on-axis jets on timescales of several years. For this reason, we encourage follow-up observations of the radiodetected sources in our sample at later epochs.

4.3. Association with More Energetic Prompt Outflows

We would like to ask: statistically speaking, are optically overluminous TDEs also more luminous in the radio band?

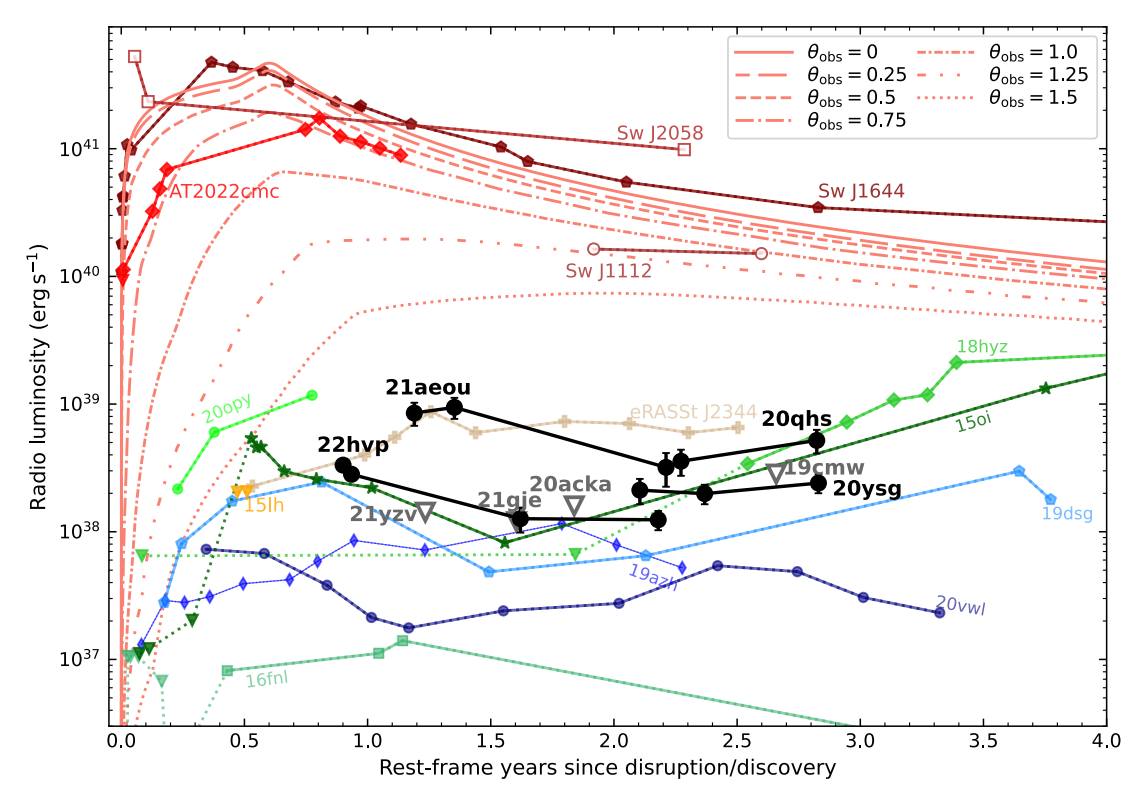


Figure 5. The black data points and gray downward triangles show VLA detections and 3σ upper limits of optically overluminous TDEs. In comparison, we show radio (~6 GHz) light curves of on-axis jetted TDEs (red lines) and other TDEs with high-cadence radio observations in the literature. We also plot 6 GHz light curves from a jet with the same properties as found for the best-fit model of Sw J1644 (P. Beniamini et al. 2023), but at different $\theta_{\rm obs}$ (see Section 4.2). References: ASASSN-150i (A. Horesh et al. 2021; A. Hajela et al. 2025), iPTF16fnl (K. D. Alexander et al. 2020; A. Horesh et al. 2021; Y. Cendes et al. 2024), AT2019azh (A. J. Goodwin et al. 2022), AT2019dsg (Y. Cendes et al. 2021, 2024), AT2020opy (A. J. Goodwin et al. 2023b), AT2020vwl (A. J. Goodwin et al. 2023a, 2025b), eRASSt J234402.9-52640 (also AT2020wjw) (A. J. Goodwin et al. 2024); Sw J1644+57 (B. A. Zauderer et al. 2011, 2013; T. Eftekhari et al. 2018), Sw J2058+05 (S. B. Cenko et al. 2012; D. R. Pasham et al. 2015; G. C. Brown et al. 2017), Sw J1112-82 (G. C. Brown et al. 2017), and AT2022cmc (I. Andreoni et al. 2022; L. Rhodes et al. 2025). We also show two overluminous TDE candidates with radio observations reported in the literature: ASASSN-15lh ($M_{g,peak} \sim -23.4$ mag; E. C. Kool et al. 2015; G. Leloudas et al. 2016; R. Margutti et al. 2017) and eRASSt J2344 ($M_{g,peak} \sim -21.8$ mag; D. Homan et al. 2023; A. J. Goodwin et al. 2024).

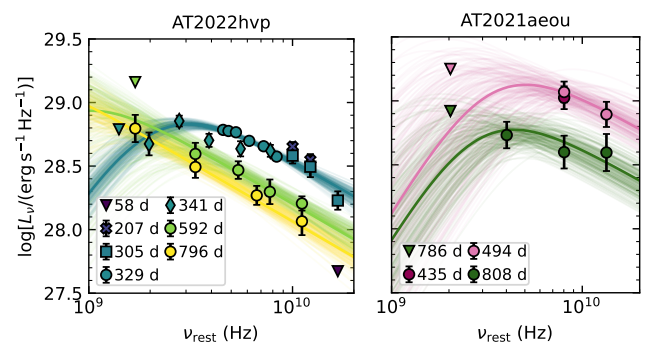


Figure 6. Radio SEDs of AT2022hvp and AT2021aeou, overplotted with the best-fit broken power-law models.

If so, this will indicate that optically overluminous TDEs might be associated with more energetic prompt²³ outflows. The inferred values of $E_{\rm eq}\sim10^{50}\text{--}10^{51}\,\rm erg}$ and $\beta\sim0.1$ for AT2022hvp and AT2021aeou (see Table 2) lie at the high end of the distribution for TDEs with radio emission attributed to prompt outflows, where $10^{47}\lesssim(E_{\rm eq}/\rm erg)\lesssim10^{51}$ and $0.01\lesssim\beta\lesssim0.1$ (see Figure 5 of A. J. Goodwin et al. 2025a).

To address this question, we compare our radio detections and upper limits obtained at $1 < (t_{rest}/yr) < 2$ for AT2022hvp,

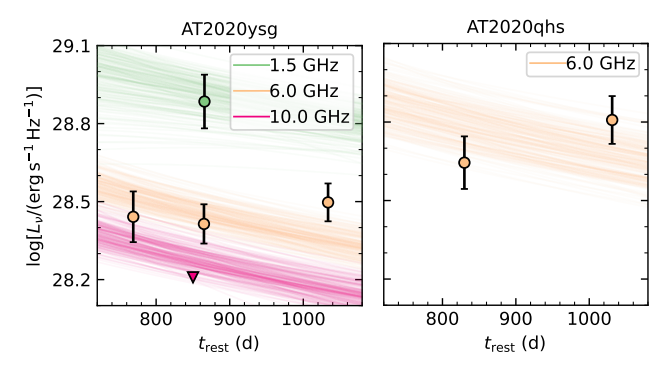


Figure 7. Radio light curves of AT2020ysg and AT2020qhs, overplotted with the best-fit Sedov–Taylor models.

AT2021aeou, AT2021gje, AT2020acka, and AT2021yzv with previously known fainter ($M_{g,peak} > -20.5$ mag) events at similar phases. We did not include AT2020qhs, AT2020ysg, and AT2019cmw in this analysis, as (1) they have observations conducted at >2 yr, which is more sensitive to delayed outflow launch (Y. Cendes et al. 2024), and (2) the origin of the radio emission in AT2020qhs and AT2020ysg is ambiguous (Section 4.1).

We construct a comparison sample of 13 TDEs with $M_{g,peak} > -20.5$ from Y. Cendes et al. (2024) (see Appendix D for details). Figure 8 shows the \sim 6 GHz radio luminosities and upper limits of our sample and the comparison sample.

²³ "Prompt" refers to a launch time that is near the optical first-light epoch.

Name	t _{rest} (days)	p	$\log u_{ m p} \ m (Hz)$	$\frac{\log L_{\nu,p}}{(\text{erg s}^{-1}\text{Hz}^{-1})}$	$\log E_{ m eq}$ (erg)	log R _{eq} (cm)	$\log n_{\rm e} ({\rm cm}^{-3})$	β	$\log M_{ m ej} \ (M_{\odot})$
AT2022hvp	329–341 592 796	$2.86^{+0.24}_{-0.21}$	$9.32^{+0.05}_{-0.04}$ < 9.50 < 9.20	29.17 ± 0.04 >28.77 >28.89	50.11 ^{+0.17} _{-0.16} >49.77 >50.10	$17.18^{+0.05}_{-0.04} \\ > 16.86 \\ > 17.23$	1.98 ± 0.21 <2.72 <2.07	0.17 ± 0.01 >0.05 >0.09	-2.27 ± 0.17 >-2.78 >-1.23
AT2021aeou	494 786–808	2.7 (fixed)	9.52 ± 0.20 $9.46^{+0.13}_{-0.18}$	$29.45^{+0.13}_{-0.11} 29.10^{+0.09}_{-0.08}$	50.96 ± 0.20 $51.02^{+0.18}_{-0.13}$	$17.09^{+0.26}_{-0.24}$ $16.98^{+0.22}_{-0.15}$	$2.22^{+0.41}_{-0.42}$ $2.18^{+0.27}_{-0.39}$	$0.12^{+0.08}_{-0.05}$ $0.06^{+0.04}_{-0.02}$	-1.12 ± 0.24 $-0.47^{+0.15}_{-0.23}$

Table 2
Radio Spectral Fit Parameters and Inferred Non-relativistic Outflow Quantities for AT2022hvp and AT2021aeou

Table 3Non-relativistic Sedov–Taylor Outflow Modeling of AT2020ysg and AT2020qhs

Name	k	$E_{\rm eq}$ (erg)
AT2020ysg	$0.63^{+0.74}_{-0.45}$	$10^{50.16\pm0.04} \left(\frac{\beta_{2.5 \text{ yr}}}{0.1}\right)^{1.407}$
AT2020qhs	$0.68^{+0.66}_{-0.48}$	$10^{50.33 \pm 0.05} \left(\frac{\beta_{2.5 \text{ yr}}}{0.1}\right)^{1.402}$

To assess whether the radio luminosity distributions of the two samples differ statistically, we performed a Bayesian analysis that accounts for censored data (i.e., upper limits). We modeled the logarithmic radio luminosities in each sample as being drawn from independent normal distributions, characterized by population means μ_1 and μ_2 and a shared standard deviation σ . Here, μ_1 corresponds to the comparison sample (dataset 1), and μ_2 to our sample of optically overluminous TDEs (dataset 2). We assumed normal priors for μ_1 and μ_2 , each centered at 38 with a standard deviation of 1 dex, and a half-normal prior on the shared standard deviation σ with a scale of 1 dex. Upper limits were treated as censored observations by including a cumulative log-probability term

$$\log P(x < x_{\lim}) = \log \Phi\left(\frac{x_{\lim} - \mu}{\sigma}\right) \tag{2}$$

in the model likelihood, where Φ is the normal cumulative distribution function. The posterior distributions were inferred using MCMC sampling as implemented in PyMC (O. Abril-Pla et al. 2023).

The posterior distribution of the mean difference, $\delta_{\mu}=\mu_1-\mu_2$, is centered at -1.2 dex, with a $94\%^{24}$ highest density interval (HDI) spanning [-2.1, -0.18]. The posterior probability that $\delta_{\mu}>0$ is 1.6%, which corresponds to a one-sided 2.1σ level of confidence in favor of $\delta_{\mu}<0$.

This result tentatively supports a connection between high optical peak luminosity and stronger radio emission on the timescale of ~ 1.5 yr. It further suggests that overluminous TDEs may be associated with more energetic prompt outflows.

A likely explanation involves the high black hole mass $(M_{\rm BH} \sim 10^8\,M_{\odot}; {\rm see}$ Table 1) found in these overluminous events. Since the tidal radius $r_{\rm T} \sim R_*(M_{\rm BH}/M_*)^{1/3}$, whereas the gravitational radius $r_{\rm g} = GM_{\rm BH}/c^2$, we have $r_{\rm T}/r_{\rm g} \sim 10(M_{\rm BH}/10^7\,M_{\odot})^{-2/3}$ for a Sun-like star. Therefore, general relativistic effects become increasingly important for disruption by higher-mass black holes. In particular, strong

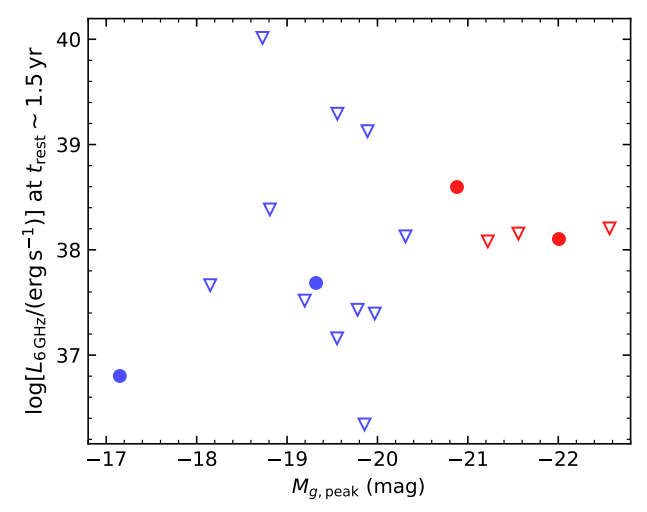


Figure 8. Radio luminosities at $t_{\rm rest} \sim 1.5$ yr for optically overluminous TDEs $(M_{g,\rm peak} < -20.8;$ shown in red) and a control sample of fainter TDEs $(M_{g,\rm peak} > -20.5;$ shown in blue). Considering both detections (solid circles) and upper limits (hollow downward triangles), our Bayesian analysis shows that our sample is brighter than the control sample at 2.1σ significance.

relativistic apsidal precession can cause enhanced mixing and collisions between the bound and unbound debris streams (P. Laguna et al. 1993; R. M. Cheng & T. Bogdanović 2014; E. Gafton & S. Rosswog 2019; T. Ryu et al. 2023). These interactions promote the circularization of bound material via stream–stream collision, while also energizing the unbound debris. The source of the outflows responsible for radio emission may be caused by either the stream–stream collision (W. Lu & C. Bonnerot 2020) or the unbound debris (J. Krolik et al. 2016). In the latter case, T. Ryu et al. (2023) showed that in extreme TDEs (defined by pericenter distances $r_p < 6r_g$), up to $\sim 1\%$ of the unbound debris's mass can reach velocities exceeding $2 \times 10^4 \, \mathrm{km \, s^{-1}}$, significantly faster than in typical TDEs hosted by lower-mass black holes.

At the same time, theoretical studies have shown that, all else being equal (e.g., black hole spin and orbital inclination), the Hills mass is larger for higher-mass stars (H.-T. Huang & W. Lu 2024; A. Mummery 2024). This raises the possibility that the stars disrupted by $M_{\rm BH} \sim 10^8\,M_{\odot}$ black holes are themselves more massive. In such cases, the disrupted star can provide a larger energy reservoir, potentially powering a more energetic outflow and hence stronger radio emission. Future demographics studies are needed to test this hypothesis.

5. Conclusion

In this paper we have presented VLA radio observations of eight optically overluminous TDEs ($M_{g,peak} < -20.8$) at $1 < (t_{rest}/yr) < 3$. The host galaxies of our sample are massive

²⁴ This is the default HDI value in the Bayesian visualization package ArviZ (R. Kumar et al. 2019). 94% is chosen as a balance between being informative and not overly wide.

 $(10^{10.6} \lesssim M_{\rm gal} \lesssim 10^{11.2})$, and the black hole masses $(10^{7.7} \lesssim M_{\rm BH} \lesssim 10^{8.3})$ are on the high end of the TDE population (Y. Yao et al. 2023).

We summarize the main conclusions below:

- 1. Radio emission is not detected in four out of the eight TDEs in our sample.
- 2. Among the four detected TDEs, their radio luminosities are in the range of 10^{38} – 10^{39} erg s⁻¹ and around two orders of magnitude fainter than those of on-axis jetted TDEs at the same phase.
- 3. We find no evidence for off-axis jets in our sample, disfavoring a connection between optically overluminous TDEs and off-axis relativistic jets.
- 4. Among the detected events, AT2022hvp and AT2021aeou show clear spectral evolution in their radio SEDs, while AT2020ysg and AT2020qhs exhibit no statistically significant variability.
- 5. The radio evolution of AT2022hvp and AT2021aeou at $1 < t_{\rm rest} < 2$ yr is consistent with synchrotron emission from non-relativistic outflows launched at the epoch of first optical light. The inferred equipartition energy is $E_{\rm eq} \sim 10^{50} 10^{51} \, {\rm erg \, s^{-1}}$, with outflow velocities of $\beta \sim 0.1c$ —these values are on the high end of TDE prompt outflow properties that have been inferred using similar approaches.
- 6. The radio emission of AT2021aeou and AT2020qhs at $2 < t_{\text{rest}} < 3$ yr may originate either from pre-existing AGN activity or from non-relativistic outflows launched by the TDEs themselves. If the former is true, our results suggest an enhanced TDE rate in radio-loud AGN.
- 7. Five TDEs in our sample have radio observations at $t_{\rm rest} \sim 1.5$ yr. When compared to the 6 GHz luminosities (including both detections and upper limits) of optically fainter TDEs with $M_{g,\rm peak} > -20.5$ mag, these overluminous TDEs exhibit systematically brighter radio emission, with a statistical significance of 2.1σ . This result supports the idea that overluminous TDEs generate more energetic non-relativistic outflows, potentially driven by strong general relativistic effects during disruptions by higher-mass black holes or the disrupted star being more massive.

Continued sensitive radio observations of this sample are needed to rule out the presence of off-axis jets with radio light curves that may rise on timescales $\gtrsim 3$ yr, and to determine the true origin of the radio emission in AT2020ysg and AT2020qhs. In addition, targeted radio monitoring of a larger sample of optically bright TDEs, with well-designed cadences, will be essential to confirm or refute the statistical trend between optical and radio luminosities.

Acknowledgments

We thank the anonymous referee for helpful comments. Y.Y. would like to thank Karamveer Kaur for helpful discussions regarding TDE rates.

Based on observations obtained with the Samuel Oschin Telescope 48 inch and the 60 inch Telescope at the Palomar Observatory as part of the Zwicky Transient Facility project. ZTF is supported by the National Science Foundation under grants No. AST-1440341, AST-2034437, and currently Award #2407588. ZTF receives additional funding from the ZTF partnership. Current members include Caltech, USA; Caltech/ IPAC, USA; University of Maryland, USA; University of California, Berkeley, USA; University of Wisconsin at Milwaukee, USA; Cornell University, USA; Drexel University, USA; University of North Carolina at Chapel Hill, USA; Institute of Science and Technology, Austria; National Central University, Taiwan, and OKC, University of Stockholm, Sweden. Operations are conducted by Caltech's Optical Observatory (COO), Caltech/IPAC, and the University of Washington at Seattle, USA.

The Gordon and Betty Moore Foundation, through both the Data-Driven Investigator Program and a dedicated grant, provided critical funding for SkyPortal. The ZTF forced-photometry service was funded under the Heising-Simons Foundation grant No. 12540303 (PI: Graham).

The National Radio Astronomy Observatory is a facility of the National Science Foundation operated under cooperative agreement by Associated Universities, Inc.

Facilities: VLA, Keck: I (LRIS), Keck: II (ESI), Hale, PO:1.2m.

Software: ArviZ (R. Kumar et al. 2019), astropy (Astropy Collaboration et al. 2022), CASA (CASA Team et al. 2022), emcee (D. Foreman-Mackey et al. 2013), LPipe (D. A. Perley 2019), matplotlib (J. D. Hunter 2007), PyMC (O. Abril-Pla et al. 2023).

Appendix A Velocity Dispersion and Black Hole Mass

In Table 1, the velocity dispersion σ_* measurements for host galaxies of AT2020acka, AT2020ysg, and AT2021yzv are taken from Y. Yao et al. (2023), and for AT2020qhs are taken from E. Hammerstein et al. (2023a). We obtained additional medium-resolution spectroscopy for the host galaxies of AT2021gje and AT2022hvp using the Echellette Spectrograph and Imager (ESI; A. I. Sheinis et al. 2002) on the Keck II telescope (see Table 4 for a log). We follow the same procedures as outlined in Y. Yao et al. (2023) to reduce the data and measure σ_* using the penalized pixel-fitting (pPXF) software (M. Cappellari & E. Emsellem 2004;

Table 4
Log of Medium-resolution Optical Spectroscopy with Keck II ESI

IAU Name	Start Date	t _{rest} (days)	Fitted $\lambda_{\text{rest}}^{\ \ a}$ (Å)	Slit Width (arcsec)	Exp. (s)	r _{extract} b (pixel)	S/N
AT2021gje	2022-03-07.6	298	3900–5300 ^a	0.5	1800	3.2	6.6
AT2022hvp	2022-11-27.6	210	5030–5600 ^a	0.75	1800	5.3	10.4

Notes.

^a Wavelength range used for spectral fitting.

b The radius used for extracting the spectrum. r_{extract} can be converted to an angular scale using a conversion factor of 0.154 per pixel.

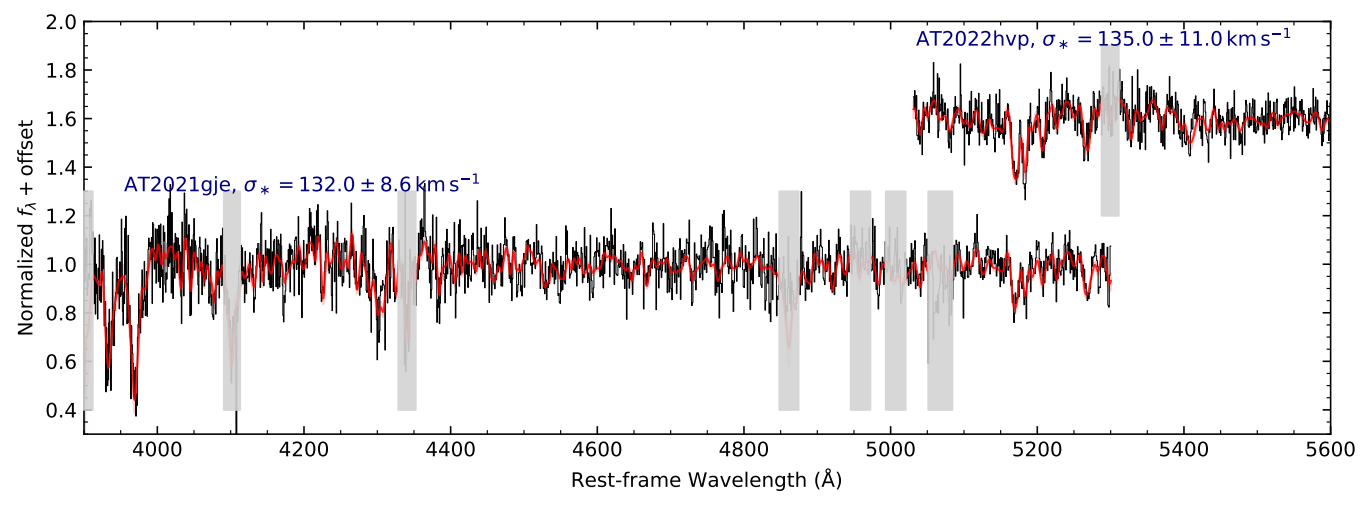


Figure 9. ESI spectrum of the host galaxies of AT2021gje and AT2022hvp (black) and the best-fit models (red).

M. Cappellari 2017). For AT2022hvp, we adopt the same rest-frame wavelength range of 5030–5600 Å for spectral fitting. For AT2021gje, due to the lower signal-to-noise ratio, we adopt a wider spectral range to include the Ca II H and K lines in the fitting. The data and best-fit models are shown in Figure 9.

We estimate the black hole mass $M_{\rm BH}$ using host galaxy scaling relations, including the $M_{\rm BH}$ – σ_* relation (J. Kormendy & L. C. Ho 2013) for six host galaxies with σ_* measurements, and the $M_{\rm BH}$ – $M_{\rm gal}$ relation (derived by J. E. Greene et al. 2020 using all types of galaxies) for the other two TDE hosts.

Appendix B Low-resolution Optical Spectroscopy of Selected TDEs

Here we provide additional follow-up spectra obtained by us for this sample (see Table 5 for a log), using the DBSP on the Palomar 200 inch Hale telescope (P200), and the Low Resolution Imaging Spectrograph (LRIS; J. B. Oke et al. 1995) on the Keck I telescope. These observations were coordinated using the *fritz.science* instance of SkyPortal (S. van der Walt et al. 2019; M. W. Coughlin et al. 2023). Instrumental setup and data reduction of DBSP and LRIS spectra are the same as outlined in Appendix B of Y. Yao et al. (2022).

Based on these, we change the spectral subtype of AT2020ysg from TDE-featureless to TDE-He (Appendix B.1), classify AT2022hvp as TDE-He (Appendix B.2), and AT2021aeou as TDE-featureless (Appendix B.3).

B.1. AT2020ysg

E. Hammerstein et al. (2023b) presented two LDT/DeVeny spectra of AT2020ysg obtained on 2020 December 6 ($t_{\rm rest} = 136 \, {\rm days}$) and 2021 January 11 ($t_{\rm rest} = 165 \, {\rm days}$). Since these spectra show blue continua and no discernible broad emission features, AT2020ysg was classified as TDE-featureless in E. Hammerstein et al. (2023b).

Here, in the upper panel of Figure 10, we show two LRIS spectra of AT2020ysg obtained at $t_{\rm rest}=141\,{\rm days}$ and 815 days. The 815 day spectrum was obtained at a sufficiently late time such that it is dominated by the host galaxy light. This allows us to reveal weak TDE spectral features in the 141 day data by comparing it with the blackbody+host model, where the host contribution is given by the 815 day spectrum. The data divided by model is shown in the bottom panel of Figure 10, where broad He II emission lines at λ 3203 and λ 4686 are evident. We note that the He II λ 3203 line is also seen in the most recent analysis of the 165 day LDT spectrum by E. Hammerstein et al. (2025). The He II λ 4686 line profile looks blueshifted and asymmetric, similar to the early-time

Table 5
Log of Low-resolution Optical Spectroscopy

IAU Name	Start Date	$t_{ m rest}$ (days)	Telescope	Instrument	Wavelength Range (Å)	Slit Width (arcsec)	Exp. (s)
AT2022hvp	2022-05-04.1	24	P200	DBSP	3410-5550, 5750-9995	1.5	450
AT2022hvp	2022-05-23.2	41	P200	DBSP	3410-5550, 5750-9995	1.5	300
AT2022hvp	2022-05-26.3	44	Keck I	LRIS	3260-10250	1.0	600
AT2022hvp	2022-10-31.6	186	Keck I	LRIS	3200-10250	1.0	$660/600^{2}$
AT2020ysg	2020-12-12.6	141	Keck I	LRIS	3200-10250	1.0	300
AT2020ysg	2023-04-21.5	815	Keck I	LRIS	3200-10250	1.0	1760
AT2021aeou	2022-07-02.2	250	Keck I	LRIS	3200-10250	1.0	1200
AT2021aeou	2022-08-02.3	264	Keck I	LRIS	3200-10250	1.0	900
AT2021aeou	2023-04-21.5	460	Keck I	LRIS	3200-10250	1.0	1760

Note.

^a Exposure times on the blue/red sides of the spectrograph.

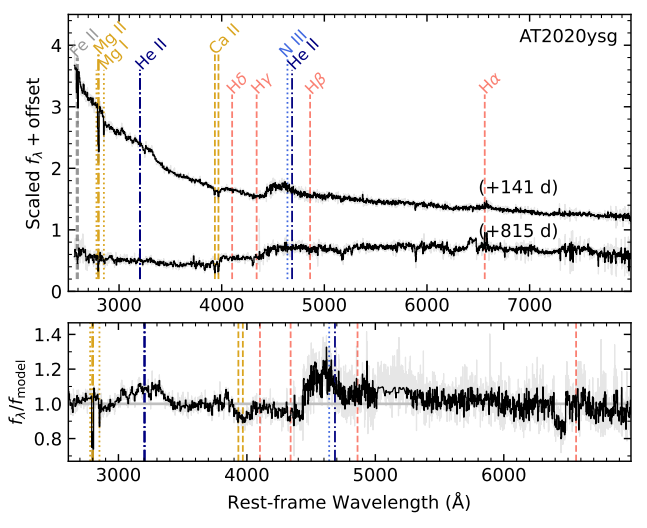


Figure 10. Upper: LRIS spectra of AT2020ysg. Bottom: The +141 days spectrum divided by a blackbody+host model, which shows signatures of broad emission lines around He II.

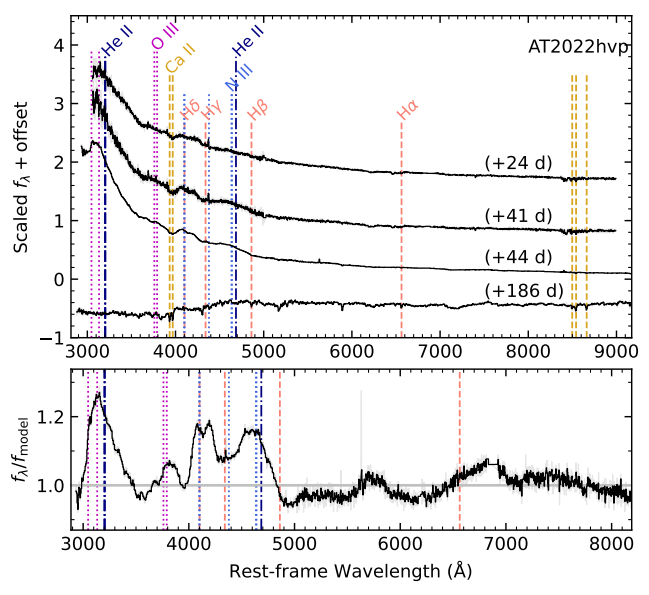


Figure 11. Upper: DBSP and LRIS spectra of AT2022hvp. Bottom: The +44 days spectrum divided by a blackbody+host model, which shows signatures of broad emission lines around O III, N III, and He II.

behavior of ASASSN-150i (T. W. S. Holoien et al. 2016). As such, we change the spectral subtype of this object from TDE-featureless to TDE-He.

B.2. AT2022hvp

AT2022hvp was classified as a TDE-He at z=0.12 using a spectrum obtained on 2022-05-06.9 ($t_{\rm rest}=27$ days) by LT/SPART (M. Fulton et al. 2022), which displays a blue continuum and broad emission features around He II and N III. The redshift of 0.12 comes from template matching. In the

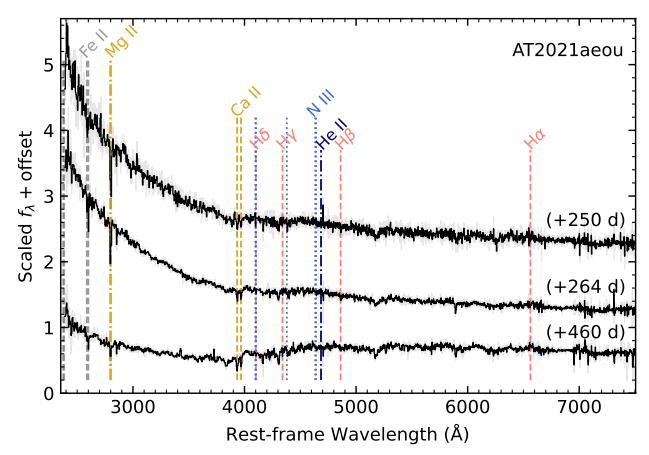


Figure 12. LRIS spectra of AT2021aeou.

upper panel of Figure 11, we show the DBSP and LRIS spectra of AT2022hvp obtained by us. We assign a more accurate redshift of z=0.112 for this TDE, as absorption lines (e.g., Ca II, H I, Na I) from the host galaxy are identified at this redshift.

Since the +44 days LRIS spectrum was obtained around maximum light, where the transient dominates, we attempt to reveal weaker line features by comparing it with a blackbody +host model, where the host is approximated by the +186 days LRIS spectrum. In the bottom panel of Figure 11, we present the data divided by model, which shows four broad emission features. The feature around He II $\lambda 4686/N$ III $\lambda \lambda 4634$, 4641 is commonly seen in optically selected TDEs. The feature at H δ/N III $\lambda 4104$ most likely comes from N III, as there are no signatures of lower-order Balmer series. The feature at ~ 3800 Å can be attributed to the O III $\lambda \lambda 3760$, 3791 Bowen fluorescence lines (P. Selvelli et al. 2007). The feature at ~ 3100 Å can be attributed to a combination of He II $\lambda 3203$ and the O III $\lambda \lambda 3047$, 3133 Bowen fluorescence lines.

We note that the intrinsic line ratio of He II $\lambda 3203/\lambda 4686$ is expected to be 0.45 under Case B recombination conditions (P. J. Storey & D. G. Hummer 1995; S. Gezari et al. 2012). The apparently enhanced strength of the He II $\lambda 3203$ line may reflect complexities in the ionization structure of the reprocessing envelope (N. Roth et al. 2016), a detailed investigation of which is beyond the scope of this work.

B.3. AT2021aeou

Figure 12 shows the LRIS spectra of AT2021aeou. We note that the optical light curve of this object exhibits a double-peaked profile (see the cyan circles in the bottom panel of Figure 4). All LRIS spectra presented here were obtained during the decline of the second peak. The transient exhibits featureless spectra.

Appendix C Additional Tables

The VLA observing log is shown in Table 6.

Table 6
Targeted VLA Observations of Overluminous TDEs

IAU Name	Date	$t_{\rm rest}$ (days)	Receiver	$ u_0 $ (GHz)	$f_ u \ (\mu m Jy)$	Array Configuration
AT2020ysg	2023-02-22.2	769	С	5.999	14.7 ± 3.3	В
	2023-06-05.9	865	X	9.999	< 8.6	BnA
	2023-06-24.9		C	5.999	13.8 ± 2.4	$BnA \to A$
	2023-06-25.8		L	1.520	40.8 ± 9.7	$BnA \to A$
	2024-01-26.3	1034	C	5.999	$16.7 ~\pm~ 2.8$	C
AT2021yzv	2023-03-12.0	451	С	5.999	<9.2	В
AT2021aeou	2023-03-18.3	435	C	5.999	$37.0 ~\pm~ 7.6$	В
	2023-06-05.9	494	L	1.520	<62.1	BnA
	2023-06-05.9		C	5.999	41.0 ± 7.7	•••
	2023-06-06.0		X	9.999	27.4 ± 6.2	•••
	2024-07-01.1	786	L	1.520	<29.1	В
	2024-07-30.1	808	S	2.999	18.9 ± 4.5	В
	2024-07-30.0		C	5.999	13.9 ± 4.1	
	2024-07-30.0		X	9.999	13.8 ± 4.6	
AT2020acka	2023-03-21.4	672	С	5.999	<7.0	В
AT2019cmw	2023-03-30.4	971	С	5.999	<4.5	В
AT2021gje	2023-04-02.3	586	С	5.999	<4.6	В
AT2022hvp	2022-06-11.0	58	Ku	15.000	<16.2	A
	2022-11-23.7	207	X	11.000	121.8 ± 12.7	C
				9.000	154.8 ± 13.0	
	2023-03-12.3	305	Ku	15.000	58.3 ± 9.7	В
			X	11.000	107.6 ± 20.3	
				9.000	131.5 ± 18.7	
	2023-04-08.1	329	C	4.103	209.6 ± 15.0	В
				4.359	205.5 ± 12.0	
				4.743	200.8 ± 8.5	
				5.511	171.8 ± 8.3	
				6.487	155.9 ± 6.7	
				7.511	129.2 ± 6.3	
	2023-04-22.0	341	L	1.264	<211.8	В
				1.776	162.6 ± 33.6	
			S	2.499	246.0 ± 24.1	
				3.499	173.4 ± 20.5	
			C	4.999	148.8 ± 20.4	
		•••	•••	6.999	143.4 ± 15.5	***
	2024-01-25.4	592	L	1.519	<498.0	C
			S	2.999	135.6 ± 27.3	
			C	4.871	101.2 ± 16.1	
				6.959	68.3 ± 15.2	
			X	9.999	55.3 ± 7.1	
	2024-09-08.6	796	L	1.52	215 ± 53	В
			S	3.00	107 ± 21	•••
			C	6.00	64 ± 11	•••
			X	10.00	$40~\pm~10$	•••
AT2020qhs	2023-04-28.9	830	С	5.999	14.7 ± 3.4	В
	2024-01-25.1	1034	C	6.000	21.4 ± 4.5	C

Note. ν_0 is the observed central frequency. f_{ν} is the observed flux density values.

Appendix D The Comparison Sample

Our goal is to compare the \sim 6 GHz radio luminosities of overluminous TDEs with those of TDEs with $M_{g,peak} > -20.5$ mag at similar postdisruption phases. For the former, we use five TDEs in our sample, each with 6 GHz observations at $1.2 < t_{\rm rest} < 1.9$ yr. For the latter, we adopt the comparison sample from Y. Cendes et al. (2024), which presents late-time radio follow-up of a systematically selected TDE sample. Unless otherwise noted, the data are taken from Y. Cendes et al. (2024).

Among the 24 TDEs in the Y. Cendes et al. (2024) sample, we exclude:

- Six events (OGLE17aaj, AT2018bsi, AT2020mot, AT2020nov, AT2020pj, and AT2020wey) whose radio emission has ambiguous origins or is likely dominated by AGN activity.²⁵
- 2. Three events (ASASSN-14ae, iPTF16axa, and AT2018lna) that lack radio observations before 2 yr.
- 3. One event (PS16dtm) with a luminous peak of $M_{g,peak} \sim -21.8$ (P. K. Blanchard et al. 2017; T. Petrushevska et al. 2023).
- 4. One event (DES14C1kia) does not have a publicly available peak optical magnitude.

This leaves a comparison sample of 13 TDEs, 10 of which have \sim 6 GHz constraints around $t_{\rm rest} \sim 1.5$ yr, including two with detections and eight with upper limits.

Two events with ~ 1.5 yr detections:

- 1. iPTF16fnl: Detected at 15.5 GHz with a flux of 151 μ Jy at $t_{\rm rest} = 1.14$ yr (A. Horesh et al. 2021), corresponding to a 6 GHz flux of 338 μ Jy assuming an optically thin spectrum with p=2.7. A 6 GHz detection at 45 μ Jy exists at $t_{\rm rest}=3.69$ yr. Interpolating in log–log space gives a 6 GHz flux of 211 μ Jy at $t_{\rm rest}=1.5$ yr.
- 2. AT2019dsg: Detected at 6 GHz with a flux of 130 μ Jy at $t_{\text{rest}} = 1.49 \text{ yr}$ (Y. Cendes et al. 2021).

Eight events with interpolatable \sim 1.5 yr upper limits:

- 1. AT2018zr: 10 GHz non-detection at <37.5 μ Jy ($t_{\rm rest}=0.19$ yr; S. van Velzen et al. 2019) and 6 GHz non-detection at <14 μ Jy ($t_{\rm rest}=2.36$ yr). We adopt a 6 GHz upper limit of <30 μ Jy at $t_{\rm rest}\sim1.5$ yr.
- 2. AT2018dyb: 19 GHz upper limit of $<43 \,\mu Jy$ at $t_{\rm rest} = 0.09 \, {\rm yr}$ (T. W. S. Holoien et al. 2020); 1.36 GHz detection at 158 μJy at $t_{\rm rest} = 2.78 \, {\rm yr}$ implies 6 GHz flux of 45 μJy (assuming p = 2.7). As the light curve rises at later times, we adopt a conservative 6 GHz upper limit of $<50 \, \mu Jy$ at 1.5 yr.
- 3. AT2018hyz: VLASS 3 GHz upper limit of < 0.45 mJy at $t_{\text{rest}} = 1.84$ yr (Y. Cendes et al. 2022).
- 4. AT2019eve: VLASS 3 GHz upper limit of < 0.497 mJy at $t_{\text{rest}} = 1.33$ yr.
- 5. AT2020neh: 15 GHz upper limit of <16 μ Jy at $t_{\rm rest} = 0.51$ yr (C. R. Angus et al. 2022); 6 GHz detection at 26 μ Jy at $t_{\rm rest} = 2.25$ yr. Given the rising light curve at later times, we adopt a 6 GHz upper limit of <26 μ Jy at 1.5 yr.

- 6. iPTF15af: 6 GHz non-detections at $t_{\text{rest}} = 0.04$ and 4.6 yr. We adopt an upper limit of $<50 \,\mu\text{Jy}$ at 1.5 yr.
- 7. AT2017eqx: 6 GHz non-detections at $t_{\rm rest} = 0.11$ yr (M. Nicholl et al. 2019) and 2.69 yr. We adopt an upper limit of $<18~\mu$ Jy at 1.5 yr.
- 8. AT2018fyk: 19 GHz non-detection of $<53 \mu Jy$ at $t_{\rm rest} = 0.32 \, \rm yr$ (T. Wevers et al. 2019), and 1.36 GHz upper limit of $<60 \, \mu Jy$ at $t_{\rm rest} = 2.65 \, \rm yr$. We adopt a 6 GHz upper limit of $<60 \, \mu Jy$ at 1.5 yr.

There are three events (AT2018hco, AT2019ehz, and AT2019teq) for which the first radio detections occur at $t_{\rm rest} > 2$ yr. Their earlier non-detections at $t_{\rm rest} < 1$ yr, combined with declining late-time light curves, prevent reliable interpolation to ~ 1.5 yr. To be conservative, we extrapolate their > 2 yr declining light curves back to $t_{\rm rest} = 1.5$ yr assuming a power-law decline of the form $f_{\nu} \propto t^{-\alpha}$ ($\alpha < 6$), and treat the result as an upper limit. This gives 6 GHz upper limits of < 1.2 mJy for AT2018hco, < 2.4 mJy for AT2019ehz, and < 9.1 mJy for AT2019teq.

ORCID iDs

Yuhan Yao https://orcid.org/0000-0001-6747-8509
Kate D. Alexander https://orcid.org/0000-0002-8297-2473
Wenbin Lu https://orcid.org/0000-0002-1568-7461
Jean J. Somalwar https://orcid.org/0000-0001-8426-5732
Vikram Ravi https://orcid.org/0000-0002-7252-5485
Ryan Chornock https://orcid.org/0000-0002-7706-5668
Raffaella Margutti https://orcid.org/0000-0003-4768-7586
Daniel A. Perley https://orcid.org/0000-0001-8472-1996
James C. A. Miller-Jones https://orcid.org/0000-0003-3124-2814

Paz Beniamini https://orcid.org/0000-0001-7833-1043 Nayana A.J. https://orcid.org/0000-0002-8070-5400 Joshua S. Bloom https://orcid.org/0000-0002-7777-216X Collin T. Christy https://orcid.org/0000-0003-0528-202X Matthew J. Graham https://orcid.org/0000-0002-3168-0139 Steven L. Groom https://orcid.org/0000-0001-5668-3507 Erica Hammerstein https://orcid.org/0000-0002-5698-8703 George Helou https://orcid.org/0000-0003-3367-3415 Mansi M. Kasliwal https://orcid.org/0000-0002-5619-4938 S. R. Kulkarni https://orcid.org/0000-0001-5390-8563 Russ R. Laher https://orcid.org/0000-0003-2451-5482 Ashish A. Mahabal https://orcid.org/0000-0003-2242-0244 Jérémy Neveu https://orcid.org/0000-0002-6966-5946 Reed Riddle https://orcid.org/0000-0002-0387-370X Roger Smith https://orcid.org/0000-0001-7062-9726 Sjoert van Velzen https://orcid.org/0000-0002-3859-8074

References

Abril-Pla, O., Andreani, V., Carroll, C., et al. 2023, PeerJ Comput. Sci., 9, e1516

Alexander, K. D., Berger, E., Guillochon, J., Zauderer, B. A., & Williams, P. K. G. 2016, ApJL, 819, L25

Alexander, K. D., Margutti, R., Gomez, S., et al. 2025, arXiv:2506.12729
Alexander, K. D., van Velzen, S., Horesh, A., & Zauderer, B. A. 2020, SSRv, 216, 81

Andreoni, I., Coughlin, M. W., Perley, D. A., et al. 2022, Natur, 612, 430
Angus, C. R., Baldassare, V. F., Mockler, B., et al. 2022, NatAs, 6, 1452
Astropy Collaboration, Price-Whelan, A. M., Lim, P. L., et al. 2022, ApJ, 935, 167

Barniol Duran, R., Nakar, E., & Piran, T. 2013, ApJ, 772, 78
Bellm, E. C., Kulkarni, S. R., Graham, M. J., et al. 2019, PASP, 131, 018002
Beniamini, P., Granot, J., & Gill, R. 2020, MNRAS, 493, 3521

 $^{^{25}}$ Five of them have observations at \sim 1.5 yr. If we include these events and treat them as upper limits, the significance of our result in Section 4.3 increases from 2.1σ to 2.5σ .

```
Beniamini, P., Piran, T., & Matsumoto, T. 2023, MNRAS, 524, 1386
Best, P. N., Kauffmann, G., Heckman, T. M., et al. 2005, MNRAS, 362, 25
Blanchard, P. K., Nicholl, M., Berger, E., et al. 2017, ApJ, 843, 106
Bloom, J. S., Giannios, D., Metzger, B. D., et al. 2011, Sci, 333, 203
Brown, G. C., Levan, A. J., Stanway, E. R., et al. 2015, MNRAS, 452, 4297
Brown, G. C., Levan, A. J., Stanway, E. R., et al. 2017, MNRAS, 472, 4469
Burrows, D. N., Kennea, J. A., Ghisellini, G., et al. 2011, Natur, 476, 421
Cappellari, M. 2017, MNRAS, 466, 798
Cappellari, M., & Emsellem, E. 2004, PASP, 116, 138
CASA Team, Bean, B., Bhatnagar, S., et al. 2022, PASP, 134, 114501
Cendes, Y., Alexander, K. D., Berger, E., et al. 2021, ApJ, 919, 127
Cendes, Y., Berger, E., Alexander, K. D., et al. 2022, ApJ, 938, 28
Cendes, Y., Berger, E., Alexander, K. D., et al. 2024, ApJ, 971, 185
Cenko, S. B., Krimm, H. A., Horesh, A., et al. 2012, ApJ, 753, 77
Cheng, R. M., & Bogdanović, T. 2014, PhRvD, 90, 064020
Christy, C. T., Alexander, K. D., Margutti, R., et al. 2024, ApJ, 974, 18
Condon, J. J., Cotton, W. D., & Broderick, J. J. 2002, AJ, 124, 675
Coughlin, M. W., Bloom, J. S., Nir, G., et al. 2023, ApJS, 267, 31
De Colle, F., & Lu, W. 2020, NewAR, 89, 101538
Dekany, R., Smith, R. M., Riddle, R., et al. 2020, PASP, 132, 038001
Eftekhari, T., Berger, E., Zauderer, B. A., Margutti, R., & Alexander, K. D.
   2018, ApJ, 854, 86
Eftekhari, T., Tchekhovskoy, A., Alexander, K. D., et al. 2024, ApJ, 974, 149
Foreman-Mackey, D., Hogg, D. W., Lang, D., & Goodman, J. 2013, PASP,
   125, 306
Fulton, M., Srivastav, S., Smartt, S. J., et al. 2022, TNSCR, 2022-1214, 1
Gafton, E., & Rosswog, S. 2019, MNRAS, 487, 4790
Gezari, S., Chornock, R., Rest, A., et al. 2012, Natur, 485, 217
Goodwin, A. J., Anderson, G. E., Miller-Jones, J. C. A., et al. 2024, MNRAS,
  528, 7123
Goodwin, A. J., Alexander, K. D., Miller-Jones, J. C. A., et al. 2023a,
    MNRAS, 522, 5084
Goodwin, A. J., van Velzen, S., Miller-Jones, J. C. A., et al. 2022, MNRAS,
   511, 5328
Goodwin, A. J., Miller-Jones, J. C. A., van Velzen, S., et al. 2023b, MNRAS,
   518, 847
Goodwin, A. J., Burn, M., Anderson, G. E., et al. 2025a, ApJS, 278, 36
Goodwin, A. J., Mummery, A., Laskar, T., et al. 2025b, ApJ, 981, 122
Graham, M. J., Kulkarni, S. R., Bellm, E. C., et al. 2019, PASP, 131, 078001
Granot, J., & Sari, R. 2002, ApJ, 568, 820
Greene, J. E., Strader, J., & Ho, L. C. 2020, ARA&A, 58, 257
Hajela, A., Alexander, K. D., Margutti, R., et al. 2025, ApJ, 983, 29
Hammerstein, E. 2021, TNSCR, 2021-1722, 1
Hammerstein, E., Cenko, B., Andreoni, I., et al. 2025, arXiv:2506.08250
Hammerstein, E., Cenko, S. B., Gezari, S., et al. 2023a, ApJ, 957, 86
Hammerstein, E., van Velzen, S., Gezari, S., et al. 2023b, ApJ, 942, 9
Heckman, T. M., & Best, P. N. 2014, ARA&A, 52, 589
Holoien, T. W. S., Auchettl, K., Tucker, M. A., et al. 2020, ApJ, 898, 161
Holoien, T. W. S., Kochanek, C. S., Prieto, J. L., et al. 2016, MNRAS, 463, 3813
Homan, D., Krumpe, M., Markowitz, A., et al. 2023, A&A, 672, A167
Horesh, A., Cenko, S. B., & Arcavi, I. 2021, NatAs, 5, 491
Huang, H.-T., & Lu, W. 2024, MNRAS, 527, 1865
Hunter, J. D. 2007, CSE, 9, 90
Janssen, R. M. J., Röttgering, H. J. A., Best, P. N., & Brinchmann, J. 2012,
   A&A, 541, A62
Jin, G., Kauffmann, G., Best, P. N., Shenoy, S., & Małek, K. 2025, A&A,
  694, A309
Kaur, K., & Stone, N. C. 2025, ApJ, 979, 172
```

Kesden, M. 2012, PhRvD, 85, 024037

Kondapally, R., Best, P. N., Duncan, K. J., et al. 2025, MNRAS, 536, 554

```
Kool, E. C., Ryder, S. D., Stockdale, C. J., et al. 2015, ATel, 8388, 1
Kormendy, J., & Ho, L. C. 2013, ARA&A, 51, 511
Krolik, J., Piran, T., Svirski, G., & Cheng, R. M. 2016, ApJ, 827, 127
Kumar, H., Berger, E., Hiramatsu, D., et al. 2024, ApJL, 974, L36
Kumar, R., Carroll, C., Hartikainen, A., & Martin, O. 2019, JOSS, 4, 1143
Laguna, P., Miller, W. A., Zurek, W. H., & Davies, M. B. 1993, ApJL,
  410, L83
Laskar, T., Berger, E., Tanvir, N., et al. 2014, ApJ, 781, 1
Law-Smith, J. A. P., Coulter, D. A., Guillochon, J., Mockler, B., &
  Ramirez-Ruiz, E. 2020, ApJ, 905, 141
Leloudas, G., Fraser, M., Stone, N. C., et al. 2016, NatAs, 1, 0002
Levan, A. J., Tanvir, N. R., Cenko, S. B., et al. 2011, Sci, 333, 199
Lu, W., & Bonnerot, C. 2020, MNRAS, 492, 686
Lu, W., Matsumoto, T., & Matzner, C. D. 2024, MNRAS, 533, 979
Margutti, R., Metzger, B. D., Chornock, R., et al. 2017, ApJ, 836, 25
Masci, F. J., Laher, R. R., Rusholme, B., et al. 2019, PASP, 131, 018003
Masci, F. J., Laher, R. R., Rusholme, B., et al. 2023, arXiv:2305.16279
Masterson, M., De, K., Panagiotou, C., et al. 2024, ApJ, 961, 211
Matsumoto, T., & Piran, T. 2023, MNRAS, 522, 4565
Mummery, A. 2024, MNRAS, 527, 6233
Mummery, A., van Velzen, S., Nathan, E., et al. 2024, MNRAS, 527, 2452
Nicholl, M., Blanchard, P. K., Berger, E., et al. 2019, MNRAS, 488, 1878
Nordin, J., Brinnel, V., van Santen, J., et al. 2019, A&A, 631, A147
Oke, J. B., Cohen, J. G., Carr, M., et al. 1995, PASP, 107, 375
Pasham, D. R., Cenko, S. B., Levan, A. J., et al. 2015, ApJ, 805, 68
Pasham, D. R., Lucchini, M., Laskar, T., et al. 2023, NatAs, 7, 88
Perley, D. A. 2019, PASP, 131, 084503
Perley, R. A., Chandler, C. J., Butler, B. J., & Wrobel, J. M. 2011, ApJL,
Petrushevska, T., Leloudas, G., Ilić, D., et al. 2023, A&A, 669, A140
Rhodes, L., Margalit, B., Bright, J. S., et al. 2025, ApJ, 992, 146
Roth, N., Kasen, D., Guillochon, J., & Ramirez-Ruiz, E. 2016, ApJ, 827, 3
Ryan, G., van Eerten, H., Piro, L., & Troja, E. 2020, ApJ, 896, 166
Ryu, T., Krolik, J., & Piran, T. 2023, ApJL, 946, L33
Sabater, J., Best, P. N., Hardcastle, M. J., et al. 2019, A&A, 622, A17
Sazonov, S., Gilfanov, M., Medvedev, P., et al. 2021, MNRAS, 508, 3820
Selvelli, P., Danziger, J., & Bonifacio, P. 2007, A&A, 464, 715
Sfaradi, I., Beniamini, P., Horesh, A., et al. 2024, MNRAS, 527, 7672
Sheinis, A. I., Bolte, M., Epps, H. W., et al. 2002, PASP, 114, 851
Stone, N. C., & Metzger, B. D. 2016, MNRAS, 455, 859
Storey, P. J., & Hummer, D. G. 1995, MNRAS, 272, 41
Sun, H., Zhang, B., & Li, Z. 2015, ApJ, 812, 33
Tchekhovskoy, A., Metzger, B. D., Giannios, D., & Kelley, L. Z. 2014,
       RAS, 437, 2744
Tchekhovskoy, A., Narayan, R., & McKinney, J. C. 2010, ApJ, 711, 50
Teboul, O., & Metzger, B. D. 2023, ApJL, 957, L9
van der Walt, S., Crellin-Quick, A., & Bloom, J. 2019, JOSS, 4, 1247
van Velzen, S., Gezari, S., Cenko, S. B., et al. 2019, ApJ, 872, 198
van Velzen, S., Gezari, S., Hammerstein, E., et al. 2021, ApJ, 908, 4
van Velzen, S., Holoien, T. W. S., Onori, F., Hung, T., & Arcavi, I. 2020,
    SRv, 216, 124
Wevers, T., Pasham, D. R., van Velzen, S., et al. 2019, MNRAS, 488, 4816
Wise, J., Perley, D., Sarin, N., et al. 2025, arXiv:2507.07380
Yao, Y., De, K., Kasliwal, M. M., et al. 2020, ApJ, 900, 46
Yao, Y., Lu, W., Guolo, M., et al. 2022, ApJ, 937, 8
Yao, Y., Lu, W., Harrison, F., et al. 2024, ApJ, 965, 39
Yao, Y., Ravi, V., Gezari, S., et al. 2023, ApJL, 955, L6
Yuan, F., & Narayan, R. 2014, ARA&A, 52, 529
Zauderer, B. A., Berger, E., Margutti, R., et al. 2013, ApJ, 767, 152
Zauderer, B. A., Berger, E., Soderberg, A. M., et al. 2011, Natur, 476, 425
```